

Article

In Silico Activity Prediction and Docking Studies of the Binding Mechanisms of Levofloxacin Structure Derivatives to Active Receptor Sites of Bacterial Type IIA Topoisomerases

Elena V. Uspenskaya ^{1,*} , Vasilisa A. Sukhanova ¹ , Ekaterina S. Kuzmina ¹, Tatyana V. Pleteneva ¹, Olga V. Levitskaya ¹ , Timur M. Garaev ²  and Anton V. Syroeshkin ¹

¹ Department of Pharmaceutical and Toxicological Chemistry, Medical Institute, RUDN University, 6 Miklukho-Maklaya St., Moscow 117198, Russia; skhnv.vasilisa@gmail.com (V.A.S.); kkuz11@inbox.ru (E.S.K.); tvplet@mail.ru (T.V.P.); levitskayavolha@gmail.com (O.V.L.); syroeshkin_av@pfur.ru (A.V.S.)

² National Research Center for Epidemiology and Microbiology Named after the Honorary Academician N. F. Gamaleya, 18 Gamaleya St., Moscow 123098, Russia; tmgaraev@gmail.com

* Correspondence: uspenskaya75@mail.ru; Tel.: +7-916-655-79-86

Abstract: The need for new antimicrobial agents (AntAg) is driven by the persistent antibiotic resistance in microorganisms, as well as the increasing frequency of pandemics. Due to the deficiency of AntAg, research aimed at developing speedy approaches to find new drug candidates is relevant. This study aims to conduct an in silico study of the biological activity spectrum as well as the molecular binding mechanisms of four structurally different forms of levofloxacin (Lvf) with bacterial topoisomerases targets of type IIA (DNA gyrase and topoisomerase IV) to enable the development of drugs with an improved characterization of the safety profile. To achieve this goal, a number of software products were used, such as ChemicPen v. 2.6, PyMol 2.5, Avogadro 1.2.0, PASS, AutoDockTools 1.5.7 with the new generation software Autodock Vina. These software products are the first to be made available for visualization of clusters with determination of ligand-receptor pair binding affinity, as well as clustering coordinates and proposed mechanisms of action. One of the real structures of Lvf, a decarboxylated derivative, was obtained with tribochemical (TrbCh) exposure. The action spectrum of molecular ligands is described based on a Bayesian probability activity prediction model (PASS software Version 2.0). Predicted and real (PMS and RMS) molecular structures of Lvf, with decreasing levels of structural complexity, were translated into descriptors via Wiener (W), Balaban (Vs), Detour (Ip), and Electropy ϵ indices. The 2D «structure-activity» diagrams were used to differentiate closely related structures of levofloxacin. PMS and RMS were visualized as 3D models of the ligand-receptor complexes. The contact regions of RMS and PMS with key amino acid residues—SER-79, DT-15, DG-1, DA-1—were demonstrated. The intra- and inter-molecular binding sites, data on free energy (affinity values, kcal/mol), the binding constant K_b (M^{-1}), and the number of clusters are presented. The research results obtained from the presented in silico approach to explore the spectrum of action find quantitative “structure-activity” correlations, and predict molecular mechanisms may be of applied interest for directed drug discovery.

Keywords: in silico methods; topological indices; Pa/Pi ratios; molecular docking; free energy of binding; type IIA topoisomerases targets; predicted and real molecular structures



Citation: Uspenskaya, E.V.; Sukhanova, V.A.; Kuzmina, E.S.; Pleteneva, T.V.; Levitskaya, O.V.; Garaev, T.M.; Syroeshkin, A.V. In Silico Activity Prediction and Docking Studies of the Binding Mechanisms of Levofloxacin Structure Derivatives to Active Receptor Sites of Bacterial Type IIA Topoisomerases. *Sci. Pharm.* **2024**, *92*, 1. <https://doi.org/10.3390/scipharm92010001>

Academic Editor: Siva Panda

Received: 13 October 2023

Revised: 13 December 2023

Accepted: 14 December 2023

Published: 20 December 2023



Copyright: © 2023 by the authors. Licensee MDPI, Basel, Switzerland. This article is an open access article distributed under the terms and conditions of the Creative Commons Attribution (CC BY) license (<https://creativecommons.org/licenses/by/4.0/>).

1. Introduction

Fluoroquinolones (FlrQs) are broad-spectrum chemotherapeutic drugs effective against Gram-positive and Gram-negative aerobic bacteria, chlamydia, and mycoplasmas. They were first introduced into clinical practice in the 1980s [1]. Despite the fact that FlrQs are considered important reserve drugs, their therapeutic relevance is controversial. Crucial to this were the 2018 overviews published by the Food and Drug Administration (FDA)

and the European Medicines Agency (EMA) on disabling adverse drug reactions (ADRs) of FlrQs in the aorta, peripheral vessels, joints, and central nervous system [2]. However, there was a significant surge of interest in FlrQs during the COVID-19 pandemic due to the shortage (approximately 63%) of antimicrobial drugs that could prevent complications after viral diseases [3].

Fluoroquinolones are classified into generations (1G–5G) based on the spectrum of biological activity, which is determined by their structural differences (QSAR effect). The introduction of a fluorine atom in C6 to the 1G fluoroquinolones—nalidixic, oxolinic, and pipemidic acids—as derivatives of the antimalarial chloroquine, resulted in 2G compounds with a broader antibacterial spectrum of activity (ciprofloxacin, norfloxacin, ofloxacin, pefloxacin, lomefloxacin) (Figure 1) [4,5].

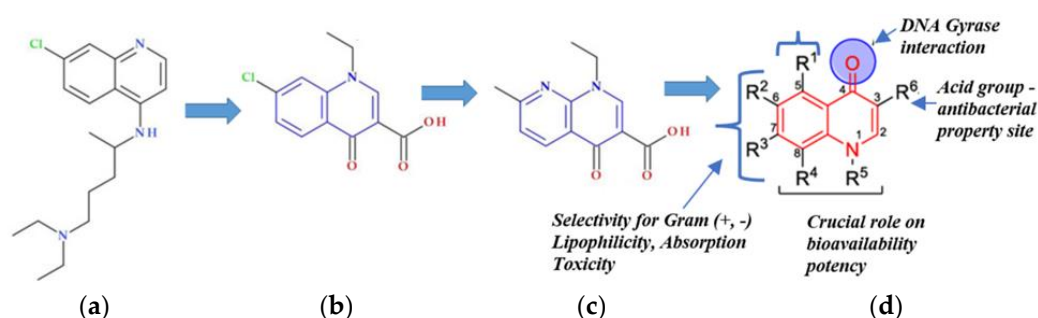


Figure 1. Evolution of the core structures of quinolone class drugs. (a) chloroquine; (b) chloro-1-ethyl-1,4-dihydro-4-oxoquinoline-3-carboxylic acid; (c) nalidixic acid; (d) FlrQs general structure. R1 = H, OH, CH₃ or –NH₂; R3 = piperazine, piperidin, pyrrolidine or azepin; R4 = CCl, CF, COMe, CHn, R5 = Alk or homocycle; R6 = COOH; R2 = Hal, CN, Alk; R4 = CCl, CF, COMe, CHn.

To date, it is known that the most crucial pharmacophore group of FlrQs consists of a central bicyclic ring with a hydrogen at the C2 position, a carboxyl group at the C3 position, and a ketone group at the C4 position. The substituents at the C7 and C8 positions have a significant influence on the efficacy, therapeutic spectrum, and safety of FlrQs (see Figure 1d). It is considered [6] that the linkage of R7 and R8 with the “A” subunit in the DNA-enzyme complex determines the direction of biological action of this class of drugs.

QSAR approaches are central to the optimization of FlrQs’ structure. The introduction of an additional fluorine atom in C8, as well as increasing the number of homo- and heterocycles, led to the development of 3G derivatives (sparfloxacin, levofloxacin). The structure was complexified by replacing the piperazine cycle with a pyrrolidine cycle and introducing an ester group, resulting in 4G derivatives (moxifloxacin, gemifloxacin). These derivatives are characterized by a longer, dose-dependent mechanism of resistance development in microorganisms, minimal inhibitory concentrations ($MIC_{90} \leq 0.25 \text{ mg} \cdot \text{L}^{-1}$), and the potential of treating nosocomial infections [7–9]. However, the increasing complexity of drug molecule structures is associated with discrepancies in the concept of an “ideal drug”, which undermines the correlation between efficacy, safety, selectivity, minimizing side effects, and broadening the therapeutic index.

Previously, it was found by *in silico* methods that, in particular, the C-3/C-4 region of quinolone keto acids is chelated by a non-catalytic Mg²⁺ ion that is coordinated by four water molecules. Common mutations in DNA gyrase observed in drug-resistant strains are thought to occur in residues that form part of the water–metal “bridge” between the enzyme and the drug [10].

In addition, the development of resistance to quinolones in various bacteria has become a clinical concern: resistance has been demonstrated for *Streptococcus pneumoniae*, as well as for isolates of methicillin-resistant *Staphylococcus aureus* (MRSA) [11].

Table 1 presents the summarized experimental and predicted data on the FlrQs’ properties of generations 1G–5G, allowing to trace the structure-dependent property evaluation.

Table 1. Chemical, physical, and biological quinolone properties values.

Molecular Weight, g·mol ⁻¹	Log Po/w	pKa (Strongest Acidic)	Water Solubility, mg·mL ⁻¹	Toxicity in Mice LD50, mg·kg ⁻¹	Microbiologic Activity/ Indications
NALIDIXIC ACID (FlrQ-1G)					
232.2	1.6	8.60	0.1	4000	Enterobacteriaceae/Uncomplicated urinary tract infections, not for use in systemic infections *
CIPROFLOXACIN (FlrQ-2G)					
331.3	0.3	6.10	<1.00	2000	Enterobacteriaceae, atypical pathogens; <i>Pseudomonas aeruginosa</i> , Pneumococci/ * and also complicated urinary tract and catheter-related infections, gastroenteritis
LEVOFLOXACIN (FlrQ-3G)					
361.4	0.7	5.50	1.44	1800	Enterobacteriaceae, atypical pathogens, streptococci. Pneumococci MIC90: 0.25–0.5 mg·L ⁻¹ /* and also community-acquired pneumonia in hospitalized patients or if atypical pathogens are strongly suspected
MOXIFLOXACIN (FlrQ-4G)					
401.4	2.9	5.49	1.15	100	Enterobacteriaceae, <i>P. aeruginosa</i> , atypical pathogens, MSSA, streptococci, anaerobes, Pneumococci. Consider for treatment of intra-abdominal infections
LEVONADIFLOXACIN (FlrQ-5G)					
360.4	0.87 **	5.94 **	0.63 **	535 **	Anti-MDR, MRSA, MDR <i>S. pneumoniae</i> , pathogenies ESKAPE, <i>P. aeruginosa</i> и <i>S. aureus</i> strains/hospital-acquired and nosocomial pneumonia, diabetic foot ulcer infections and skin and soft tissue infections, acute otitis eterna (swimmer's ear)

*—uncomplicated urinary tract infections, not for use in systemic infections, **—predicted.

Progress in combinatorial chemistry has led to the development of new FlrQs (5G), approved by the FDA and EMA in the last decade—nemonoxacin, finafloxacin, zabofloxacin, levonadifloxacin, lascufloxacin, delafloxacin. These fluoroquinolones have demonstrated potent activity against penicillin-resistant and multi-drug-resistant (MDR) pneumococcus and anaerobes, while maintaining their activity against aerobes [12]. The structure of FlrQs and quinolones QNs (5G) differs from other generations by the content of 1 to 3 fluorine atoms (lascufloxacin), the combination of halogens—fluorine and chlorine (delafloxacin)—the complete absence of halogen atoms, for example, in nemonoxacin, as well as several chiral centers, which determine the optical and pharmacological activity of the isomers (Figure 2) [13].

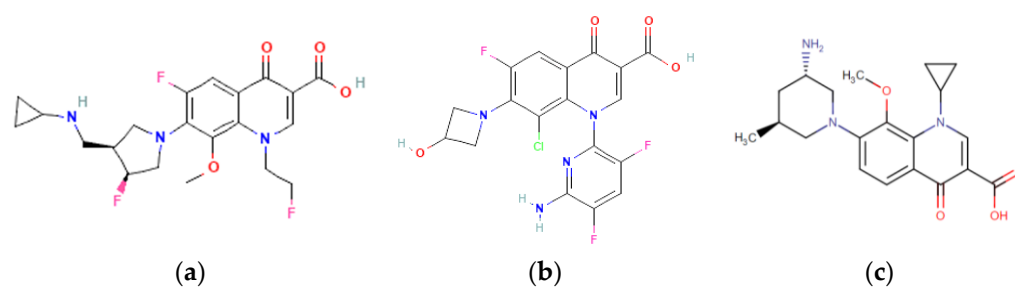


Figure 2. Chemical structure of newer approved antibacterial QN (5G). (a)—lascufloxacin, (b)—delafloxacin, (c)—nemonoxacin.

In connection with the discovery of new FlrQs, cases of manifestation by the considered drug group have been reported, showing “non-classical” biological activities such as anti-HIV-1 integrase [14], cannabinoid receptor-2 agonist/antagonist [15], anxiolytic agents, antiischemic activities, antiviral effects, etc., are continually injecting new enthusiasm towards this scaffold of drug [16]. This highlights the significance of the question regarding the correlation between the “structure-activity” relationship. This relationship is based on different mechanisms of low molecular biological activity of xenobiotics in the quinolones group. The activity depends on the nature and spatial arrangement of functional groups.

It is known that one approach to developing new drugs with improved pharmacokinetic and pharmacodynamic characteristics is to isolate and study the properties of metabolites produced through drug biotransformation. In this case, the original drug substance functions as a prodrug. Fluoroquinolones undergo biochemical modification to a lesser extent. The main metabolites are demethylated structure, *N*-oxide, and formyl derivatives, which do not have significant pharmacological activity. Levofloxacin is mainly excreted unchanged in the urine [17].

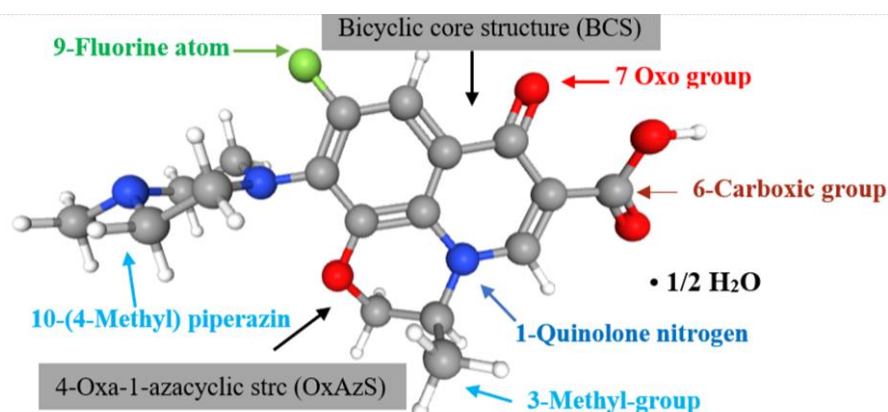
In this task, the importance of new strategies in modeling the biological activity of substances is increasing. These strategies include direct modeling to recreate the structure of the ligand-receptor complex, as well as evaluating conformation and mutual affinity using *in silico* QSAR and molecular docking methods. *De novo* design, which aims to recreate the hypothetical structure of target molecules, enables the design of the poses of low-molecular-weight ligands in the active binding site with the receptor. This is achieved by minimizing the repulsion energy of groups (steric factor) and maximizing the binding energy [18].

The aim of this work is to apply *in silico* methods to study the biological activity and patterns of changes in the properties of various molecular graphs, and to predict the molecular mechanisms of binding of levofloxacin structural derivatives to bacterial type IIA topoisomerase.

2. Materials and Methods

2.1. Fluoroquinolone Samples

In this work, the high purity ($\geq 99, 9\%$) levofloxacin hemihydrate (Lv $\cdot 1/2$ H $_2$ O) pharmaceutical substance produced by the Jiangsu Aimi Tech Co., Ltd. (Jiangsu China) is presented (Figure 3).



(3S)-9-Fluoro-3-methyl-10-(4-methylpiperazin-1-yl)-7-oxo-2,3-dihydro-7H-pyrido[1,2,3-de][1,4]benzoxazine-6-carboxylic acid hemihydrate

Figure 3. 3D chemical structure depiction of levofloxacin hemihydrate [19].

2.2. QSAR

Biological activity was predicted based on Quantitative Structure-Activity Relationships (QSAR) analysis of PMS and RMS structures in CHP и MOL, ChemDesk using the software ChemicPen v. 2.6 (<https://cetramax-chemicpen.software.informer.com>, accessed on 21 October 2022) [20]. Real and predicted molecular structures (RMS and PMS) were translated into unified characteristic structural descriptors through numerical (topological) indices (TI): Wiener (W), Balaban (Bc), Detour (Ip) and Electropy (E), describing various physicochemical and biological properties of molecular graphs (Tables 2 and S1) [21].

Table 2. Topological indices.

Topological Index	Definition	Equation
Wiener (W)	the shortest distances sum between all pairs of vertices in G graph	$W = 0.5 \sum_{i=1}^n \sum_{j=1}^n (d)_{ij}$ where d_{ij} is the shortest distance between vertices i and j
Balaban (J)	the average distance-sum connectivity index	$J = \frac{m}{m-n+2} \sum_{uv \in E(G)} \frac{1}{\sqrt{w(u) \cdot w(v)}}$ where n and m are the cardinalities of the vertex and the edge set of G , respectively, and $w(u)$ (resp. $w(v)$) denotes the sum of distances from u (resp. v) to all the other vertices of G
Detour (Ip)	the sum of the upper triangle of the detour Δ matrix	$I_p = \sum \Delta_{ij}$ where the i, j -th entry Δ_{ij} denotes the longest path between vertices i and j of the underlying graph ($i, j = 1, 2, \dots, N$) where N denotes the number of vertices
Electropy (Ie)	the sum of the squares of the atomic nuclear charges divided by the square of the number of atoms in the molecule minus one	$\epsilon = 1b \left(\frac{p_a}{p_i} \right)$ p_a and p_i represent the probabilities for the occurrence of an a priori event and i -posteriori event. The larger the Ie index value, the more electropositive the molecule is.

The topological (W) index allowed us to compare the size and shape of the graph-carbon skeletons of saturated hydrocarbon fragments in the studied Lvf structures [22]. The (J) index of a connected graph G was used to calculate the distance matrix for molecules containing multiple bonds [23]. The longest distances between atoms of the molecular

graph were considered in the traversal matrix I_p , while the matrix I_e accounted for the influence of spatial and electronic factors [24].

2.3. PASS

PASS (Prediction of Activity Spectra for Substances) Online (<http://www.way2drug.com/passonline/>, accessed on 21 June 2022)—is a software product that allows predicting the biological activity of loaded PMS and RMS using Pa criteria (to be active) и Pi (to be inactive) [25]. The maximum activity value is taken as the ratio $P_a/P_i = 1$, while a quantitative property value close to zero ($P_a/P_i \rightarrow 0$) was considered “inactive”. PASS is based on the analysis of molecular structure profiles based on MNA descriptors (Multilevel neighborhoods of atoms) and a Bayesian probabilistic model for predicting the biological activity of molecular ligands [26]:

$$P(A_k | C) = P(C | A_k) \cdot P(A_k) / P(C), \quad (1)$$

where $P(A_k | C)$ is the probability of structure C provided that the chemical compound has activity A_k , $P(A_k)$ is the a priori probability of activity A_k , $P(C)$ is the a priori probability of structure C .

In PASS, the notion of equivalence is of particular importance: structures are considered equivalent if they are described by the same set of MNA descriptors [27,28].

2.4. Software of Molecular Docking

Generation of real molecular structures of the leader compound—levofloxacin—as well as predicted molecular structures, including various bioisosters and degradation products, was performed using the molecular editor Avogadro 1.2.0 (https://avogadro.cc/releases/avogadro_120/, accessed on 15 June 2016) [29]. Using this improved molecular editor based on quantum mechanical structure calculation, further geometric optimization of small ligand molecules was carried out.

The identified interactions between low-molecular-weight ligands and the structure of topoisomerase IIA were visualized using PyMol 2.5 (<https://pymol.org/2/>, accessed on 1 October 2022) [30,31].

The crystal structure of the topoisomerase IIA-DNA-6-FQ complex originating from a bacterial species (*Streptococcus pneumoniae* topo IV-DNA-levofloxacin, PDB ID:3k9F) were utilized based on the available validation protocol wwPDB X-ray Structure Validation Summary Report (https://pdj.org/emnavi/disp.php?a=arch.valrep_pdb_sum.3k9f, accessed on 15 October 2009).

The preliminary preparation of the protein model included removal of the solvate environment, addition of polar hydrogen molecules and was performed in the AutoDock-Tools 1.5.7 program [32,33]. Adding hydrogen atoms to the protein structure taken from the PDB and optimizing their positions were the most crucial steps [34].

Achilles Blind Docking Server (<https://bio-hpc.ucam.edu/achilles/>, accessed on 25 January 2023), whose working framework is AutoDock Vina, was used to determine the pose of the crystallographic structure of topoisomerase IIA with Lvf structure derivatives ligand and to calculate the binding energy values [35,36].

AutoDock Vina achieves a speed up of approximately two orders of magnitude compared to the molecular docking software previously developed, while also significantly improving the accuracy of the binding mode predictions. Further speed up is achieved from parallelism, by using multithreading on multicore machines. AutoDock Vina automatically calculates the grid maps and clusters the results in a way that is transparent to the user [37,38].

2.5. Equipment for Tribochemical Processing

The one of the real (6-decarboxylated) Lvf chemical structure derivatives were obtained by tribochemical method based on the intensive impact and cutting loads on the solid [39]. For this purpose, a Stegler LM-250 milling mechanoactivator with a brush motor (Shenzhen

Bestman Instrument CO., Ltd., Shenzhen, China), rotation speed 28,000 rpm, power 13 kW, was used. The steps of tribochemical impact on the levofloxacin powder included loading of the substance suspension into the grinding vessel about ½ volume and discharging of the sample substance after 21 min of continuous mechanical impact (Figure S1).

2.6. Fourier Transform IR Spectroscopy

To obtain the vibrational spectra of the levofloxacin RMS, a Fourier transform infrared spectroscopy (FTIR) (Agilent Cary 630, Santa Clara, CA, USA) with a transmission attachment was used in the spectral range from 4000 to 400 cm^{-1} .

2.7. Optical Microscopy (OM)

The microscope with a special binocular attachment (Altami BIO 2, Saint Petersburg Russia) with magnification 10× (linear field of view 20 mm) was used to determine the particles' morphologies.

2.8. Statistical Data Processing

All statistical data processing was performed using Student's t-test, as well as using the one-way analysis of variance (ANOVA) in the Origin Pro 2021 software (<https://www.originlab.com/2021>, accessed on 15 January 2021)). The differences were considered statistically significant at $p < 0.05$.

3. Results and Discussion

3.1. Structure-Activity Relationship Study

To predict the biological activity profile of levofloxacin derived structures, the following approaches were used: in silico modification to obtain derivatives of predicted Lvf structures and tribochemical effects on the drug substance powder to obtain various Lvf real derivatives.

Experimenting In Silico (Chemicpen, PASS Online, ChemDescript)

Table 3 presents the «structure-activity» analysis for a sample of homogeneous predicted Lvf derivatives, presented in decreasing order of complexity of the investigated FlrQ-3G structures. For this purpose, we applied the approach of sequentially detaching the most important functional groups from the basic structure to determine the spectrum of antimicrobial activity (Figures S2 and S3, Scheme S1).

Table 3. In silico prediction of the biological activity spectrum of levofloxacin derivatives.

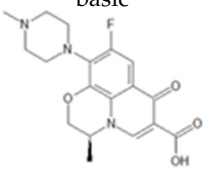
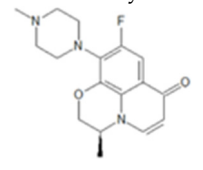
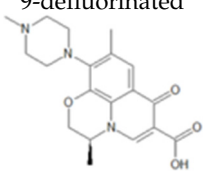
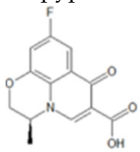
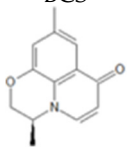
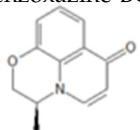
№	Lvf Structure Derivatives	Prediction Spectra of Biological Activity (Pa)						
		Ing TopII ^{1*}	Ing DNAS ^{2*}	SDAc ^{3*}	QnAnMc ^{4*}	AntBc ^{5*}	AntTt ^{6*}	Ing CYP1 A2 ^{7*}
1	basic 	0.851	0.818	0.797	0.653	0.636	0.559	0
2	6-decarboxylated 	0.699	0.620	0.811	0.351	0.818	0.589	0.716

Table 3. Cont.

№	Lvf Structure Derivatives	Prediction Spectra of Biological Activity (Pa)						Ing CYP1A2 ^{7*}
		Ing TopII ^{1*}	Ing DNAS ^{2*}	SDAc ^{3*}	QnAnMc ^{4*}	AntBc ^{5*}	AntTt ^{6*}	
3	9-defluorinated 	0.699	0.620	0.811	0.351	0.818	0.589	0.716
4	10-depyperazine 	0.756	0.634	0.753	0.495	0.575	0.347	0.467
5	4-benzoxazine-BCS 	0.472	0.487	0.699	0.095	0.426	0.455	0.518
6	5-dehydro-4-benzoxazine-BCS 	0.302	0.405	0.638	0.035	0.271	0.453	0.424

^{1*}—type II DNA topoisomerase inhibitor that prevents ATP-dependent cleavage of both DNA chains of microbial cells. ^{2*}—inhibitor of reparative and replicative DNA synthesis of microbial cells. ^{3*}—smart drug activities (Nootropics). ^{4*}—quinolone antimicrobial agent. ^{5*}—antibacterial agent. ^{6*}—antitumor activity. ^{7*}—cytochrome P-450 CYP1A2 isofor inhibitor.

As can be seen from the data tables, with probability $Pa > 0.8$, the basic structure 1 predictably demonstrates quinolone antimicrobial activity, conditioned by the mechanisms of type IIA topoisomerase inhibition and DNA synthesis of the bacterial cell. According to [40], this proves that with a probability of 80% an error will be made rejecting the assumption that the molecule of analyzed Lvf exhibits this type of activity.

The prediction of the biological activity spectrum for structures 2–4, in the absence of a carboxyl group at C6, a covalently bound fluorine atom at C9, and methylpiperazine at C10, is of significant interest. There is a persistent high probability ($Pa \geq 0.7$) of antibacterial activity due to the properties of Ing TopII and Ing DNA synthesis. Additionally, the PASS software prediction suggests the manifestation of smart drug (nootropics) and cytochrome P-450 CYP1A2 inhibitor properties, which are not typical for FlrQ, with 0.5–0.8 of Pa range. Moreover, the predicted activities for quinolone structures 2 and 3 demonstrate consistent quantitative confidence for all species listed in the Table 3. This may indicate the importance of the identical contribution of structural descriptors in the form of -COOH and -F groups to the «structure-activity» relationship for fluoroquinolones, which was confirmed in the literature by the example [41], as well as their MNA equivalence.

Further extensive modification of Lvf (structures 5 and 6) with variants only preserve the basic 4-benzoxazine-BCS results in the highest probability of completely losing of quinolone antimicrobial activity ($Pa < 0.1$), as well as all presented tabular species mentioned, except for the smart drug properties ($Pa \sim 0.7$). The results of the nootropic activity prediction for the basic oxa-azatricyclo structure of quinolone obtained by PASS

may serve as a foundation for the development of novel drugs that enhance the metabolism of neuronal cells of the central nervous system [42].

In order to establish the dependence between the predictive spectrum of biological activity and the structure of related Lvf predicted compounds, we calculated integral and differential topological indices that are known for their high discriminating ability.

Figure 4 shows two-dimensional (2D) diagrams demonstrating the regularities in the character of changes in properties when considering different molecular graphs.

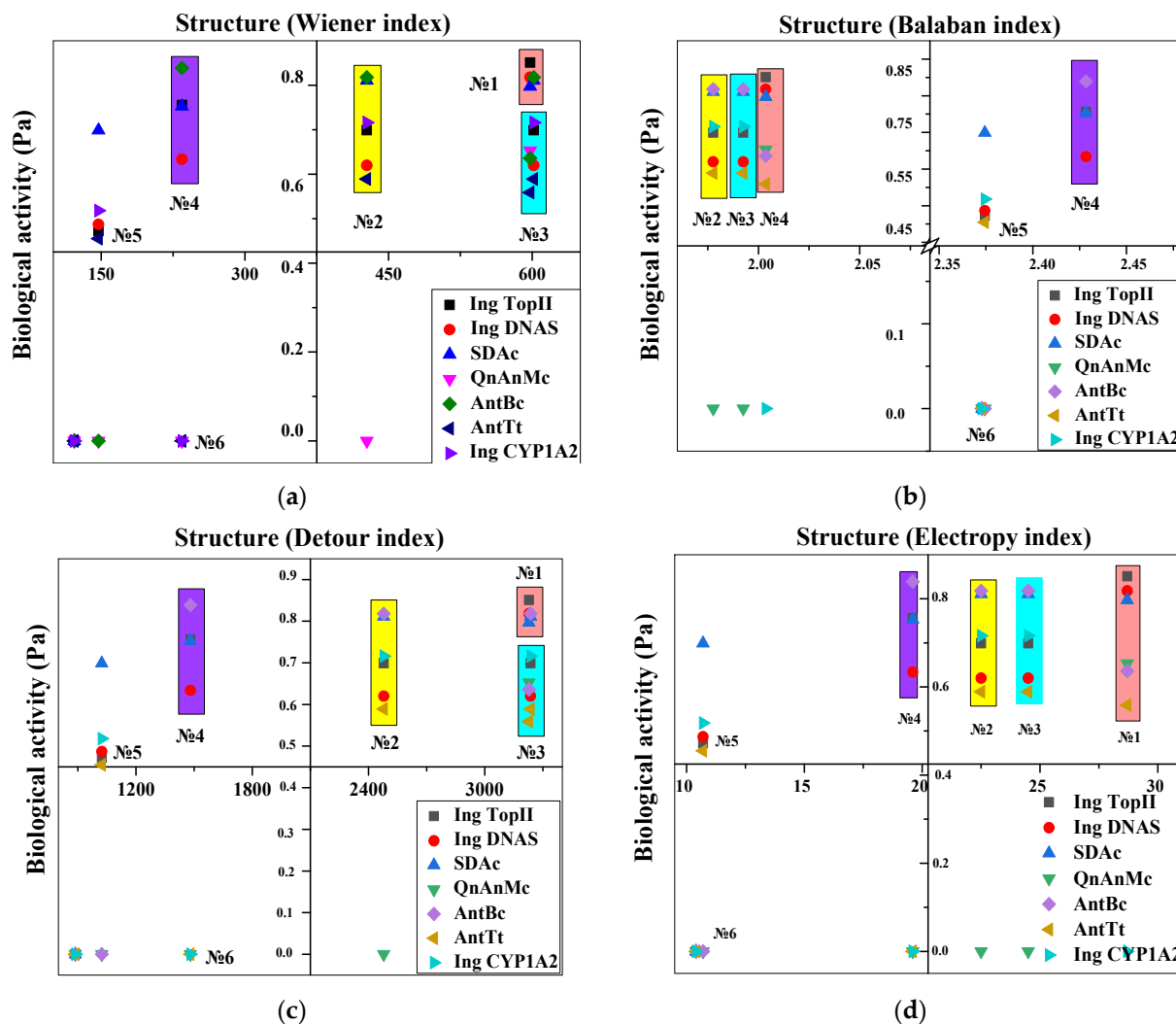


Figure 4. 2D diagrams of «structure-biological activity» relationship for the considered levofloxacin’s predicted (№ 2–№6) derivatives relative to the real (№1) Lvf’s structure. (a) Wiener index; (b) Balaban index; (c) Detour index; (d) Electropy index. The area structures: red—basic, blue—9-defluorinated, yellow—6-decarboxylated, violet—10-depyperazine. On the inserts—biological activity spectrum of predicted levofloxacin derivatives.

As can be seen, structures №1 (basic/real) and №3 (9-defluorinated) correspond to a cluster of points that are responsible for the manifestation of different types of biological activity; they occupy the same area relative to the OX axis (Figure 4a). Taking into consideration the fact that the calculation of the Wiener index (W) is based on the distance matrix related to the size and shape of the graph, we can assume that, from a quantitative characterization perspective of molecular structures, there are no differences between structures №1 and №3. The structure №2, corresponding to the 6-decarboxylated derivative of Lvf, occupies a distinct region, indicating the specificity of the invariant set of the molecular graph.

The consecutive destruction of the fluoroquinolone molecule (structures №4 and №5) leads to the formation of stable dots in a distinct region that does not intersect with the basic Lv_f structure when the nitrogenous base is removed in FIQns molecules. Structure № 6 is characterized by a scattering of dots over regions without any specific positions being manifested. This directly indicates a violation of the «structure-activity» relationship. A comparable result for all analyzed structures was obtained when calculating the Detour (I_p) indices (Figure 4c). The use of indices that are the sum of simpler indices (see Table 2) leads to a lower degree of degeneracy and improves efficiency in identifying chemical structures [43].

Of some interest is the 2D diagram that describes the distribution of prognostic biological activity values depending on the index. These calculations are based on the concept of the center of the graph J(G) (Figure 4b). It can be seen that each of the predicted structures presented occupies a distinct position in the diagram field. At the same time, in one area, there are close equivalent structures №1–№3, while the 10-depyperazine structure (№4) occupies a separate area. The Balaban index (J) indicates a relatively low level of degeneracy.

Topological indices correlate satisfactorily with both steric parameters (such as molecular volume, molecular surface area, etc.) and electronic parameters (including ionization potentials, electron affinity, polarizability, spin densities, etc.). With the assistance of quantum chemical calculations, one can acquire supplementary information regarding the electron density distribution in a molecule by utilizing the I_e electropy index (Figure 4d).

Thus, the comparison of topological indices for analyzing related modified fluoroquinolone structures has not only revealed the presence of a «structure-activity» correlation, but also the functional interdependence of topological indices (TIs) among themselves. The Balaban and Electropy indices are the most informative, low degenerate TIs for describing the structures and properties of Lv_f derivatives.

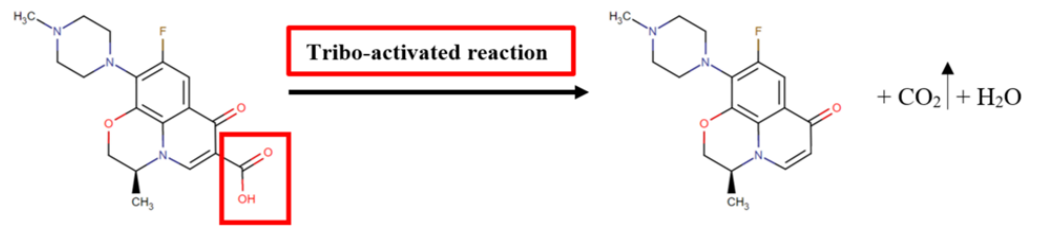
All the presented 2D diagrams demonstrate the similarity of the structure and properties to the basic structure of the defluorinated derivative. Decarboxylation and defluorination of the Lv_f structure significantly reduce the prognostic FIQns antimicrobial activity by twofold. Additionally, these processes result in the emergence of other “non-classical” biological activities, such as inhibition of the cytochrome P-450 CYP1A2 isoform. However, the best model for effectively differentiating predicted equivalent structures of levofloxacin is the decarboxylated derivative (dLv_f), based on the representation of topological indices of TI (see Figures 1 and 4).

To obtain the real 6-decarboxylated structure of Lv_f, we utilized the method that relies on tribochemical processes.

3.2. Experimentation Using Tribochemical Processes

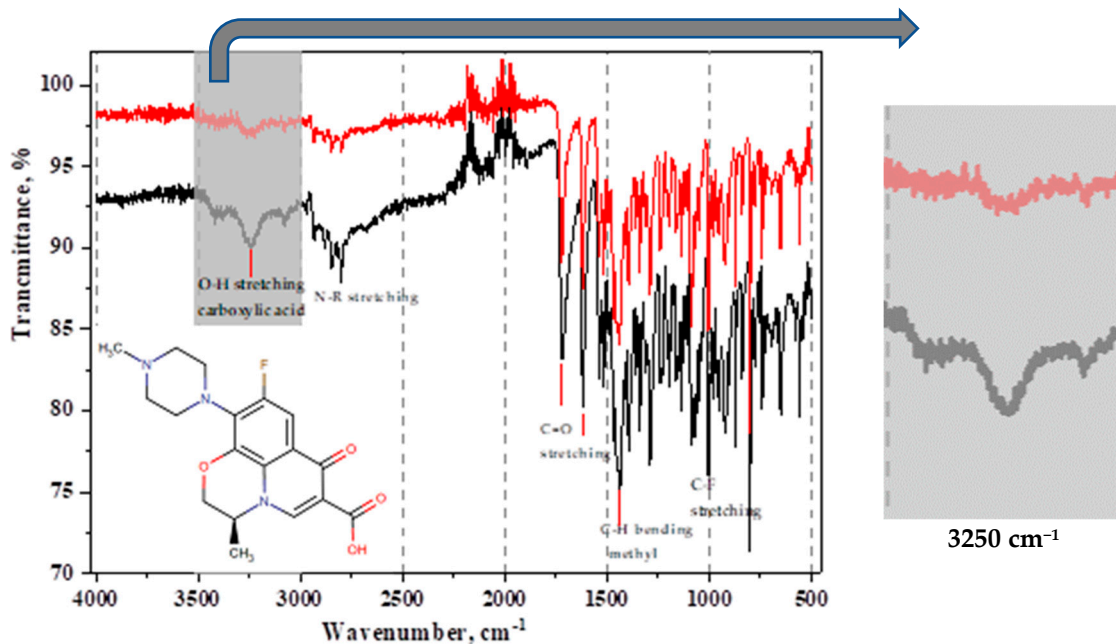
High local temperatures created at surface friction contacts lead to the formation of catalytic centers that determine chemical activity. According to the catalytic approach described in [44], there are sequential processes of low-energy electron emission, their interaction with molecules at the surface friction boundary, combined with thermionic emission. Obviously, a specific combination of physical and chemical phenomena leads to the initiation of a heterogeneous chemical reaction (Scheme 1).

Based on the patterns observed in non-thermal chemical reactions, which are accompanied by high-intensity friction, deformation, and static mechanical stress applied to the solid, the resulting product, a decarboxylated derivative of Lv_f, was analyzed using optical methods of physicochemical analysis (Figures 5 and S4).

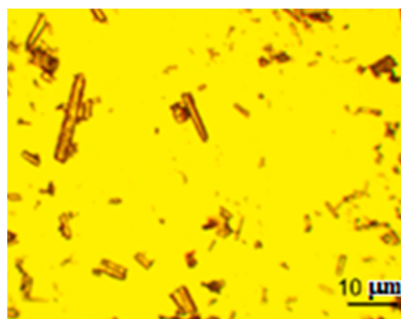


Scheme 1. Tribochemical synthesis procedure of levofloxacin derivative. Conditions: 65 °C, 21 min, 13 kW of mechanical activator power.

The results of this study demonstrate changes in solid-state properties after the tribochemical impact. Specifically, degeneration of the needle shape of crystals is observed, a large fraction of particles falls within the size group $d = 5 \mu\text{m}$. Covalent bonds that have been deformed due to high-intensity tribochemical impact exhibit a bathochromic shift of maxima in the FT-IR spectrum. The vibration erosion is manifested by the complete disappearance of the characteristic high-frequency valence vibrations of -OH-hydroxyl in the carboxyl group in the 3250 cm^{-1} region.



(a)



(b)



(c)

Figure 5. Cont.

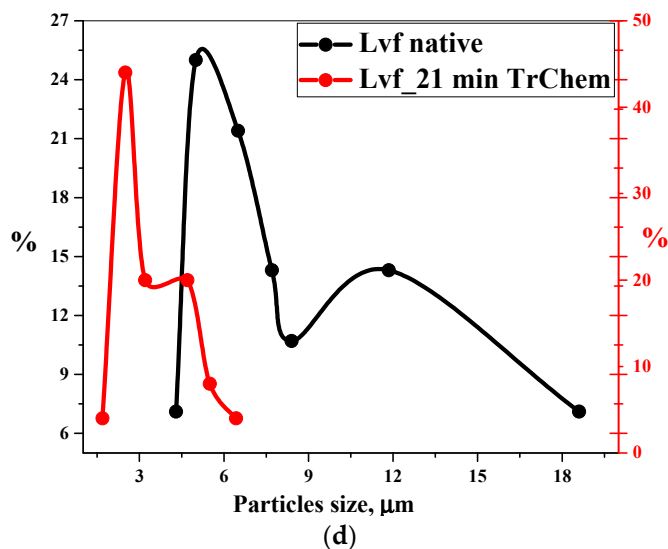


Figure 5. A series of methods for qualitative, morphometric and granulometry analysis of Lvf substance samples before and after tribochemical treatment. (a) FT–IR spectrometry, black—Lvf native, red—tribo-activated Lvf (on a separate inset – region of O–H bond vibrations in the carboxyl group); (b,c) – optical microscopy (OM) of Lvf native and triboactivated substances, respectively; (d) OM granulometry for: black—Lvf native, red—triboactivated Lvf.

3.3. Binding Modes Prediction and Molecular Modeling

Molecular docking was performed to predict the binding of real and predicted derivatives of levofloxacin to specific regions of type IIA topoisomerase target proteins [45]. The inhibitor molecule was docked in the quinolone resistance determining region (QRDR) of genes, which is attributed to a high frequency of substitutions in the QRDR region of the GyrA subunit of DNA gyrase [46–48].

Visualization between RMS, Compounds of PMS, and DNA Gyrase II

The most advantageous orientations and conformations of low-molecular-weight ligands in the active center of protein-receptor binding for the formation of stable supramolecular complexes were demonstrated. The fixed spatial (3D) positions of the ligand-receptor pair for structures №1–№4 (see Table 3), which demonstrated a satisfactory QSAR dependence according to the results of the *in silico* experiment, are presented in Figure 6.

The validation of molecular docking results was conducted using the RMSD method. For the structure of 3K9F, native docking was successful: the RMSD between the docked lowest energy ligand pose and its crystallized pose is 0.986 Å. This value indicates a low deviation (less than 2 Å) between the predicted and reference structures, suggesting that the docking method applied in this study effectively predicts the spatial conformation of molecular complexes.

According to data (see Figure 6), the contact regions of the RMS and PMS low-molecular-weight ligands with key amino acid residues in the protein-receptor structure—SER-79 (serine), DT-15 (deoxythymidine), DG-1 (deoxyguanosine), DA-1 (deoxyadenosine)—are represented by intra- and inter-molecular binding sites of –OH and C=O of the carboxyl group at C6, C=O at C7, and C–O–C in 4-benzoxazine-BCS residue by hydrogen bonding.

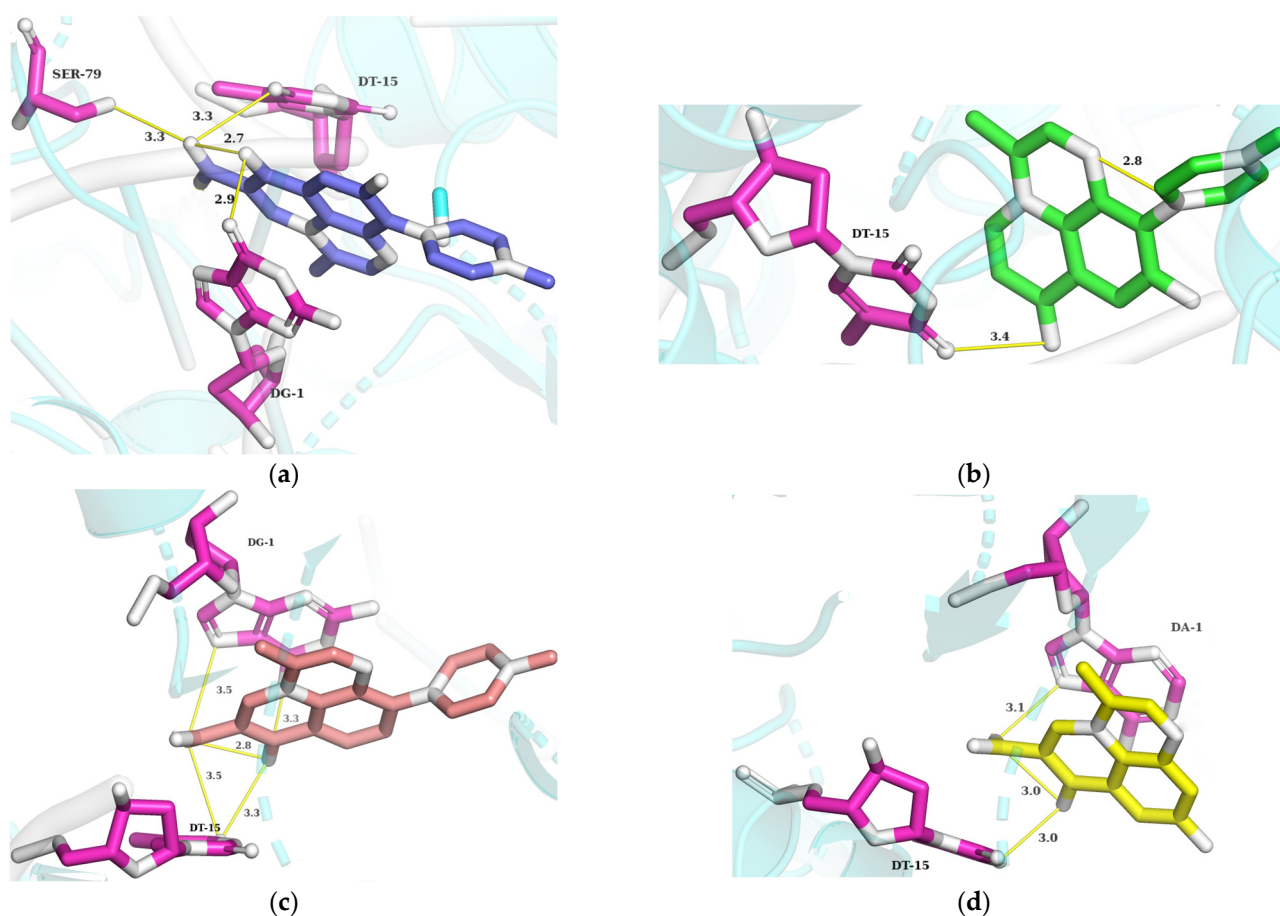


Figure 6. Docking conformations obtained for different molecular structures of Lvf with specific regions of type IIA topoisomerase target proteins (with distances Å). H-bonds shown as yellow lines; non-polar hydrogen atoms have been removed for clarity [49]. (a)—basic Lvf; (b)—6-decarboxylated derivative; (c)—9-defluorinated derivative; (d)—10-depyperazine derivative.

As can be seen from the presented 3D models, the pair with the native carboxylated ligand exhibits the largest number of bonds in spatial positions (see Figure 6a). Also, a number of amino acid residues are involved in the complexes formed between the target protein—bacterial type IIA topoisomerases—and the 9-defluorinated derivative and 10-depyperazine derivative of Lvf (see Figure 6c,d). All these factors contribute to stronger binding of the ligand to the active site of the receptor protein [50].

At the decarboxylated RMS position, the carbonyl group of the ligand and the deoxythymidine residue (in lactim form) participate in the formation of inter-molecular bonds in the complex. The oxygen atom -O- in the 4-benzoxazine-BCS residue forms an intra-molecular bond with hydrogen at C2 in the 4-methylpiperazin-1-yl substituent.

For geometry-based ligand-receptor binding, the Autodock Vina employs an empirical scoring function, including two Gauss terms and repulsion, hydrophobic, and hydrogen bonds [51,52]. Table 4 shows the scoring functions of characterization to approximately predict the binding affinity of a ligand-receptor pair after they dock. The average contribution of each interaction to the final predicted binding energy (affinity, kcal/mol) is expressed in parts of a percent.

In the scoring function, a weighted sum of steric interactions are in the first three terms in Table 4, and hydrophobic interaction between hydrophobic atoms and hydrogen bonding (the last two terms in Table 4).

Table 4. Empirical scoring function weights and terms.

Ligand	Steric Interaction			Non-Steric Interaction		Affinity Values, kcal/mol
	Gauss 1	Gauss 2	Repulsion	Hydrophobic Attraction	Non-Directional Hydrogen Bond	
basic Lvf	7.50	91.97	0.16	0.29	0.08	−9.7
9-defluorinated	7.67	91.74	0.17	0.31	0.11	−9.4
6-decarboxylated	7.35	92.17	0.12	0.33	0.03	−8.9
10-depyperazine	8.66	90.84	0.19	0.19	0.12	−8.6

The binding constants of the protein-ligand system is predicted via AutoDock Vina software (autodock.scripps.edu. Date of access: 15 May 2016) that converts the affinity energy values (kcal/mol) into K_b according to the following equation:

$$\Delta G_{bind}^0 = -RT \ln K_b \quad (2)$$

$$K_b = \exp \exp \left(\frac{-\Delta G_{bind}}{RT} \right) \quad (3)$$

$$K_b = K_d^{-1} \quad (4)$$

where ΔG_{bind}^0 represents the free energy of “protein-ligand” binding, kcal/mol, R is the universal gas constant (8.314×10^{-3} kJ/K·mol), T is 298 K (25 °C), K_b is the binding constant, M^{-1} , and K_d is the dissociation constant, M.

For solved docking positions, clustering results are available in the form of coordinates of the ligand position in the active center of the target protein near the global minimum of the energy of the formed complex. The binding poses characterized by the lowest docking energy in order to identify the highest ranked clusters were analyzed after docking using the AutoDockTools 1.5.7 program (see Section 2.4). These results allow for the prediction of the binding mechanism (Figure 7, Table 5).

The clustering histogram shows the number of binding conformations at different binding energies. A number of clusters with high population indicates, as a rule, that docking has been successfully performed [53,54].

The clustering results reveal significant differences between the predicted molecular structure of 10-depyperazine and the original structure of levofloxacin and other PMS derivatives. The highest value of the Gibbs free energy, along with a larger number of clusters and conformations of low-molecular-weight ligands in the binding center, indicate unsatisfactory outcomes in locating the low-energy minimum of the complex. The 9-defluorinated structure closely resembles the initial levofloxacin structure in terms of the spectrum of low-energy minima and the K_b values. Here, we can observe a correlation with the QSAR results of the in silico experiment (see Figure 4).

As expected, the structure of the 6-decarboxylated derivative obtained by the TrbCh method, which has the fewest number of bonds to the single amino acid residue DT-15, is characterized by lower docking accuracy (see Table 4). This indicates that the properties of fluoroquinolones depend on the carboxylated structure (see Figures 1 and 2).

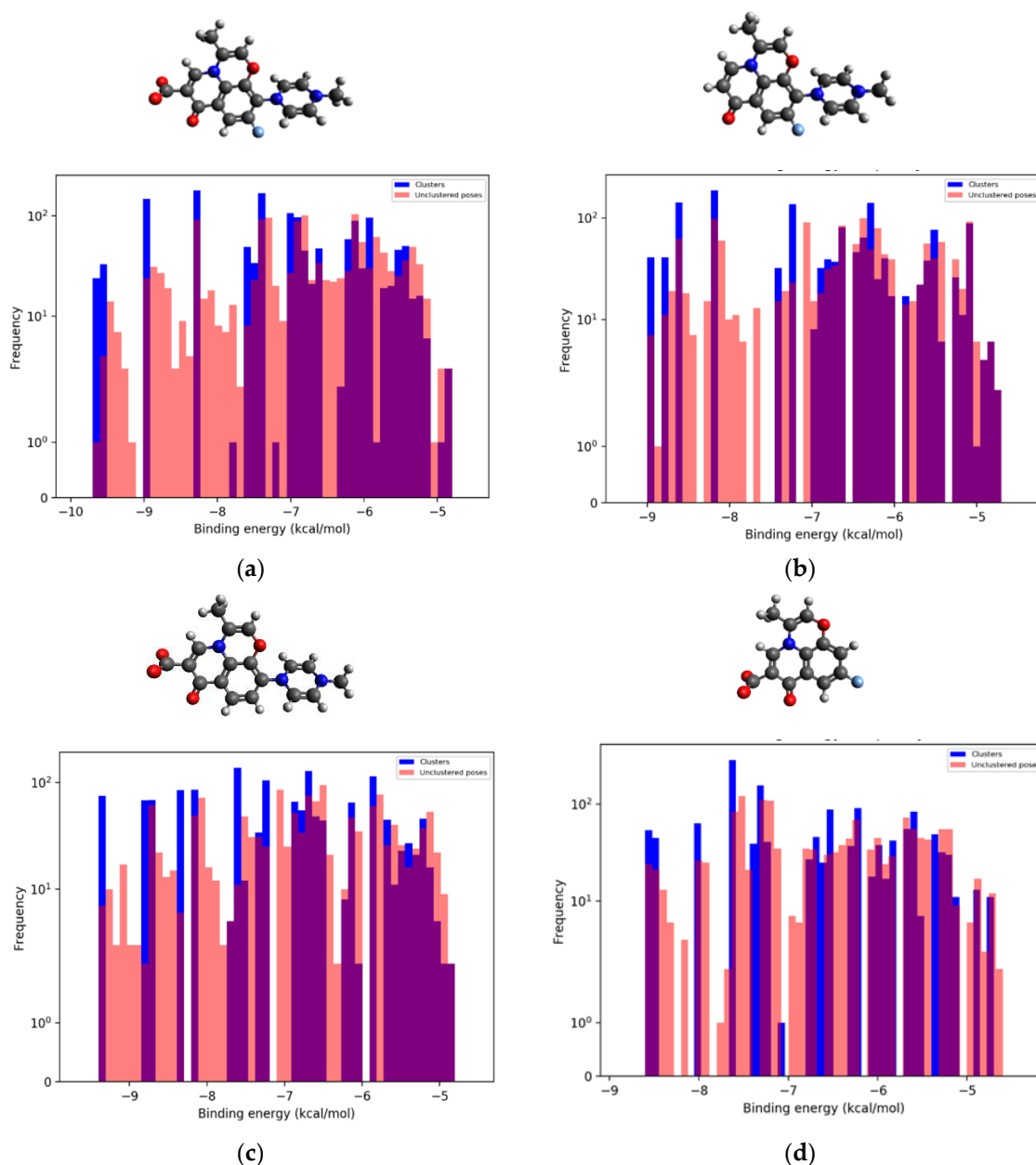


Figure 7. Clustering diagrams. (a) basic levofloxacin; (b) 6–decarboxylated derivative; (c) 9–defluorinated derivative (d) 10–depyperazine derivative (the purple areas of the diagrams show the number of low population clusters). On the upper insets—the ligands images after processing the molecular editor Avogadro 1.2.0; atoms of elements are highlighted by color: dark gray—C, light gray—H, blue—N, red—O.

Table 5. Clustering data.

Poses in Cluster	Best Pose	Binding Site Coordinates	$K_b \cdot 10^5, M^{-1}$
	basic levofloxacin		
24	592	(−22.18, 50.92, −37.92)	1.31
33	1201	(−39.00, 54.45, −38.88)	
69	232	(−18.02, 26.50, −36.81)	
	9-defluorinated		
36	982	(−22.25; 51.62, −38.84)	1.30
39	591	(−39.10, 54.89, −38.22)	
68	173	(−18.43, 27.23, −36.66)	

Table 5. Cont.

Poses in Cluster	Best Pose	Binding Site Coordinates	$K_b \cdot 10^5, M^{-1}$
	6-decarboxylated		
41	1228	(−39.16, 54.97, −38.91)	1.29
41	1001	(−22.00, 51.04, −38.77)	
66	258	(−17.54, 26.57, −36.31)	
	10-depyperazine		
54	1223	(−38.84, 54.74, −37.11)	1.28
45	592	(−22.03, 51.80, −37.31)	
37	985	(−18.27, 55.28, −25.49)	

4. Conclusions

In this work, we demonstrate the use of *in silico* approaches for searching for quantitative structure-activity correlations using the example of real (RMS) and predicted (PMS) structures of levofloxacin. The biological activity profile of levofloxacin derivatives was evaluated in descending order of complexity of their structure in comparison with the original levofloxacin based on a Bayesian probabilistic model. It was shown that the absence of a carboxyl group in the structure of the molecule significantly reduces the prognostic antimicrobial activity of FIQns by twofold. In addition, these processes lead to the appearance of other “non-classical” biological activities, such as inhibition of cytochrome P-450 isoform CYP1A2. Balaban and Electropy indices are shown to be the most informative and weakly degenerate topological indices to describe and distinguish between RMS and PMS derivatives of Lvf. Judging from the presented 2D diagrams, the structures that closely resemble each other are the basic and defluorinated Lvf. Using new generation molecular docking software products (AutoDockTools 1.5.7 with the new generation software Autodock Vina), the biologically active candidate molecules of levofloxacin selected by QSAR analysis were visualized as 3D models of ligand-receptor complexes. On the basis of the empirical scoring function, the final predicted binding energy (affinity, kcal/mol), the binding constants K_b (M^{-1}), as well as data from the clustering diagrams, the proximity of the structure of 9-defluorinated Lvf to the initial structure of levofloxacin was demonstrated. The results obtained are of practical importance for the introduction of drugs into pharmacy with predetermined properties derived from a known lead drug and a certain active center of the target protein [55].

Supplementary Materials: The following supporting information can be downloaded at <https://www.mdpi.com/article/10.3390/scipharm92010001/s1>: Figure S1: FTIR spectrum (a) and Solidstate ^{13}C NMR spectrum (b) of FA; Figure S2: SEM images (a–d), EDX spectra and the distribution of elements in powders on aluminum foil (e), and FA appearance (f), respectively; Figure S3: The Pa for the RMS of. Figure S4: Optical Microscope granulometry of RMS of Lvf. Table S1: Standard deviations of the results of measurements of the fluorescence of the FA solution; Scheme S1: PASS (Prediction of Activity Spectra for Substances) Online for RMS and PMS of Lvf.

Author Contributions: Conceptualization, E.V.U. and V.A.S.; methodology, E.V.U., A.V.S. and T.V.P.; investigation, E.V.U., V.A.S. and E.S.K.; data curation, V.A.S. and T.M.G.; formal analysis, E.V.U.; writing—original draft preparation, E.V.U.; writing—review and editing, A.V.S. and T.V.P. All the authors discussed the results and commented on the manuscript. All authors have read and agreed to the published version of the manuscript.

Funding: This research has been supported by the RUDN University Strategic Academic Leadership program grant number 033320-0-000.

Institutional Review Board Statement: Not applicable.

Informed Consent Statement: Not applicable.

Data Availability Statement: The data are available upon reasonable request.

Acknowledgments: The authors would like to thank Vladimir B. Sulimov—the head of the Research computing center laboratory, Lomonosov Moscow State University, for advice on molecular modeling.

Conflicts of Interest: The authors declare no conflict of interest.

Abbreviations

AntA	antimicrobial agents
ANOVA	one-way analysis of variance
MCh	mechanochemistry
MAct	mechanoactivation
TrbCh	tribochemical
QNs	quinolones
FlrQs	fluoroquinolones
SMComplex	supramolecular complex
FDA	Food and Drug Administration
EMA	The European Medicines Agency
ADR	adverse drug reactions
TrbCh	tribochemical
Lvf-Hh	levofloxacin hemihydrate
QSAR	quantitative structure-activity relationship
QRDR	Quinolone resistance determining region
MIC	minimal inhibitory concentrations
MRSA	Methicillin-Resistant <i>Staphylococcus aureus</i>
MDR	Penicillin-resistant and multi-drug-resistant <i>Streptococcus pneumonia</i>
RMS	real molecular structures
PMS	predicted molecular structures
PLD	predicted levofloxacin derivatives
dLvf	11-decarboxylated levofloxacin
TI	topological index
FT-IR	Fourier transform IR spectroscopy
PASS	Prediction of Activity Spectra for Substances
MNA	Multilevel neighborhoods of atoms
LALLS	low-angle laser light scattering
OM	optical microscopy
DSA	dynamic strain aging
2D-LS	two-dimensional dynamic backscattering
ChRS	chemometric reference sample
ETEC	enterotoxigenic <i>Escherichia coli</i>
RMSD	Root Mean Square Deviation

References

- Vidyavathi, M.; Srividya, G. A review on ciprofloxacin: Dosage form perspective. *Int. J. App. Pharm.* **2018**, *10*, 6–10. [CrossRef]
- Center for Drug Evaluation and Research. FDA Updates Warnings for Oral and Injectable Fluoroquinolone. U.S. Food and Drug Administration. 2018. Available online: <https://www.fda.gov/drugs/drug-safety-and-availability/fda-drug-safety-communication-fda-updates-warnings-oral-and-injectable-fluoroquinolone-antibiotics> (accessed on 12 May 2016).
- Dey, B.K.; Myrsing, E.; Amin, R.; Alam, F.; Rahman, M.; Gogol, P.; Afroz, T. A ripple effect of COVID-19 pandemic on shortage of medicinal products and its impact on patient care. *Int. J. App. Pharm.* **2021**, *13*, 364–370. [CrossRef]
- Rusu, A.; Munteanu, A.C.; Arbănași, E.M.; Uivarosi, V. Overview of side-effects of antibacterial fluoroquinolones: New drugs versus Old Drugs, a step forward in the safety profile? *Pharmaceutics* **2023**, *15*, 804. [CrossRef] [PubMed]
- Spencer, A.C.; Panda, S.S. DNA Gyrase as a Target for Quinolones. *Biomedicines* **2023**, *11*, 371. [CrossRef] [PubMed]
- Millanao, A.R.; Mora, A.Y.; Villagra, N.A.; Bucarey, S.A.; Hidalgo, A.A. Biological Effects of Quinolones: A Family of Broad-Spectrum Antimicrobial Agents. *Molecules* **2021**, *26*, 7153. [CrossRef] [PubMed]
- Ray, G.T.; Baxter, R.; DeLorenze, G.N. Hospital-level rates of fluoroquinolone use and the risk of hospital-acquired infection with ciprofloxacin-nonsusceptible *Pseudomonas aeruginosa*. *Clin. Infect. Dis.* **2005**, *41*, 441–449. [CrossRef] [PubMed]
- Kishii, R.; Yamaguchi, Y.; Takei, M. In vitro activities and spectrum of the novel fluoroquinolone lascufloxacin (KRP-AM1977). *Antimicrob. Agents Chemother.* **2017**, *61*, e00120-17. [CrossRef]

9. Bhagwat, S.S.; Nandanwar, M.; Kansagara, A.; Patel, A.; Takalkar, S.; Chavan, R.; Periasamy, H.; Yeole, R.; Deshpande, P.; Bhavsar, S.; et al. Levnadifloxacin, a Novel Broad-Spectrum Anti-MRSA Benzoquinolizine Quinolone Agent: Review of Current. *Drug Des. Dev. Ther.* **2019**, *13*, 4351–4365. [CrossRef]
10. Bridle, M.J.; Janesko, B.G. Computational Study of Fluoroquinolone Binding to $Mg(H_2O)_N^{2+}$ and Its Applicability to Future Drug Design. *Int. J. Quantum Chem.* **2017**, *117*, e25428. [CrossRef]
11. Bush, N.G.; Diez-Santos, I.; Abbott, L.R.; Maxwell, A. Quinolones: Mechanism, Lethality and Their Contributions to Antibiotic Resistance. *Molecules* **2020**, *25*, 5662. [CrossRef]
12. Rusu, A.; Lungu, I.-A.; Moldovan, O.-L.; Tanase, C.; Hancu, G. Structural characterization of the millennial antibacterial (fluoro)quinolones—Shaping the fifth generation. *Pharmaceutics* **2021**, *13*, 1289. [CrossRef] [PubMed]
13. US National Library of Medicine, National Center for Biotechnology Information, PubChem. Available online: <https://pubchem.ncbi.nlm.nih.gov/compound/Lascufloxacin> (accessed on 23 June 2023).
14. Dayam, R.; Al-Mawsawi, L.Q.; Zawahir, Z.; Witvrouw, M.; Debyser, Z.; Neamati, N. Quinolone 3-carboxylic acid pharmacophore: Design of second generation HIV-1 integrase inhibitors. *J. Med. Chem.* **2008**, *51*, 1136–1144. [CrossRef] [PubMed]
15. Stern, E.; Muccioli, G.G.; Millet, R.; Goossens, J.-F.; Farce, A.; Chavatte, P.; Poupaert, J.H.; Lambert, D.M.; Depreux, P.; Hénichart, J.-P. Novel 4-oxo-1,4-dihydroquinoline-3-carboxamide derivatives as new CB2 cannabinoid receptors agonists: Synthesis, pharmacological properties and molecular modeling. *J. Med. Chem.* **2006**, *49*, 70–79. [CrossRef] [PubMed]
16. Manera, C.; Benetti, V.; Castelli, M.P.; Cavallini, T.; Lazzarotti, S.; Pibiri, F.; Saccomanni, G.; Tuccinardi, T.; Vannacci, A.; Martinelli, A.; et al. Design, synthesis, and biological evaluation of new 1,8-naphthyridin-4(1H)-on-3-carboxamide and quinolin-4(1H)-on-3-carboxamide derivatives as CB2 selective agonists. *J. Med. Chem.* **2006**, *49*, 5947–5957. [CrossRef] [PubMed]
17. Zhu, L.; Zhang, Y.; Yang, J.; Wang, Y.; Zhang, J.; Zhao, Y.; Dong, W. Prediction of the pharmacokinetics and tissue distribution of levofloxacin in humans based on an extrapolated PBPK model. *Eur. J. Drug Metab. Pharmacokinet.* **2016**, *41*, 395–402. [CrossRef] [PubMed]
18. Krishnan, S.R.; Bung, N.; Vangala, S.R.; Srinivasan, R.; Bulusu, G.; Roy, A. De novo structure-based drug design using Deep Learning. *J. Chem. Inf. Model.* **2022**, *62*, 5100–5109. [CrossRef] [PubMed]
19. US National Library of Medicine, National Center for Biotechnology Information, PubChem. Available online: <https://pubchem.ncbi.nlm.nih.gov/compound/Levofloxacin> (accessed on 23 June 2023).
20. Informer Technologies, Inc. Available online: <https://chemicpen.software.informer.com/> (accessed on 21 October 2022).
21. Randić, M.; Sabljic, A.; Nikolić, S.; Trinajstić, N. A rational selection of graph-theoretical indices in the QSAR. *Int. J. Quant. Chem.* **1998**, *34*, 267–285. [CrossRef]
22. Balaban, A.T. Topological indices and their uses: A new approach for the coding of alkanes. *J. Mol. Struct. THEOCHEM* **1988**, *165*, 243–253. [CrossRef]
23. Gopika, S.; Lakshmi, A.; Aiswarya, P.D.; Rajendran, S. On the Detour Based Indices. *Math. Stat. Eng. Appl.* **2022**, *71*, 951–966.
24. Fang, W.; Liu, W.-H.; Liu, J.-B.; Chen, F.-Y.; Hong, Z.-M.; Xia, Z.-J. Maximum Detour–Harary Index for Some Graph Classes. *Symmetry* **2018**, *10*, 608. [CrossRef]
25. Filimonov, D.A.; Lagunin, A.A.; Glorizova, T.A. Prediction of the Biological Activity Spectra of Organic Compounds Using the Pass Online Web Resource. *Chem. Heterocycl. Compd.* **2014**, *50*, 444–457. [CrossRef]
26. Fomenko, A.E.; Sobolev, B.N.; Filimonov, D.A.; Poroikov, V.V. Use of structural MNA descriptors for designing profiles of protein families. *Biophysics* **2003**, *48*, 595–605.
27. Dmitriev, A.V.; Rudik, A.V.; Karasev, D.A.; Pogodin, P.V.; Lagunin, A.A.; Filimonov, D.A.; Poroikov, V.V. In silico prediction of drug–drug interactions mediated by cytochrome P450 isoforms. *Pharmaceutics* **2021**, *13*, 538. [CrossRef] [PubMed]
28. Filimonov, D.A.; Druzhilovskiy, D.S.; Lagunin, A.A.; Glorizova, T.A.; Rudik, A.V.; Dmitriev, A.V.; Pogodin, P.V.; Poroikov, V.V. Computer-aided prediction of biological activity spectra for chemical compounds: Opportunities and limitation. *Biomed. Chem. Res. Meth.* **2018**, *1*, e00004. [CrossRef]
29. Hanwell, M.D.; Curtis, D.E.; Lonie, D.C.; Vandermeersch, T.; Zurek, E.; Hutchison, G.R. Avogadro: An advanced semantic chemical editor, visualization, and Analysis Platform. *J. Cheminform.* **2012**, *4*, 17. [CrossRef] [PubMed]
30. Maschietto, F.; Allen, B.; Kyro, G.W.; Batista, V.S. MDiGest: A Python package for describing allostery from molecular dynamics simulations. *J. Chem. Phys.* **2023**, *158*, 215103. [CrossRef] [PubMed]
31. Rosignoli, S.; di Paola, L.; Paiardini, A. PyPCN: Protein contact networks in PyMOL. *Bioinformatics* **2023**, *39*, btad675. [CrossRef]
32. Morris, G.M.; Huey, R.; Lindstrom, W.; Sanner, M.F.; Belew, R.K.; Goodsell, D.S.; Olson, A.J. AutoDock4 and AutoDockTools: Automated docking with selective receptor flexibility. *J. Comput. Chem.* **2009**, *30*, 2785–2791. [CrossRef]
33. Eberhardt, J.; Santos-Martins, D.; Tillack, A.F.; Forli, S. AutoDock Vina 1.2.0: New Docking Methods, Expanded Force Field, and Python Bindings. *J. Chem. Inf. Model.* **2021**, *61*, 3891–3898.
34. Sulimov, V.B.; Kutov, D.C.; Taschilova, A.S.; Ilin, I.S.; Tyrtysnikov, E.E.; Sulimov, A.V. Docking Paradigm in Drug Design. *Curr. Top. Med. Chem.* **2021**, *21*, 507–546. [CrossRef]
35. Vieira, T.F.; Sousa, S.F. Comparing AutoDock and Vina in Ligand/Decoy Discrimination for Virtual Screening. *Appl. Sci.* **2019**, *9*, 4538. [CrossRef]

36. Zhou, X.; Ling, M.; Lin, Q.; Tang, S.; Wu, J.; Hu, H. Effectiveness Analysis of Multiple Initial States Simulated Annealing Algorithm, A Case Study on the Molecular Docking Tool AutoDock Vina. *IEEE/ACM Trans. Comput. Biol. Bioinform.* **2023**, *1*–12. Available online: <https://ssrn.com/abstract=4120348>; <http://dx.doi.org/10.2139/ssrn.4120348> (accessed on 26 May 2022). [[CrossRef](#)] [[PubMed](#)]
37. Trott, O.; Olson, A.J. AutoDock Vina: Improving the speed and accuracy of docking with a new scoring function, efficient optimization, and multithreading. *J. Comput. Chem.* **2010**, *31*, 455–461. [[CrossRef](#)] [[PubMed](#)]
38. Agarwal, R.; Smith, J.C. Speed vs Accuracy: Effect on Ligand Pose Accuracy of Varying Box Size and Exhaustiveness in AutoDock Vina. *Mol. Inform.* **2023**, *42*, e2200188. [[CrossRef](#)] [[PubMed](#)]
39. Uspenskaya, E.; Simutina, A.; Kuzmina, E.; Sukhanova, V.; Garaev, T.; Pleteneva, T.; Koldina, A.; Kolyabina, E.; Petrov, G.; Syroeshkin, A. Exploring the effects of cramped-impact-type mechanical action on active pharmaceutical ingredient (levofloxacin)—Prospects for pharmaceutical applications. *Powders* **2023**, *2*, 464–483. [[CrossRef](#)]
40. Lagunin, A.; Stepanchikova, A.; Filimonov, D.; Poroikov, V. PASS: Prediction of activity spectra for Biologically Active Substances. *Bioinformatics* **2000**, *16*, 747–748. [[CrossRef](#)] [[PubMed](#)]
41. He, Q.Q.; Zhang, X.; Yang, L.M.; Zheng, Y.T.; Chen, F. Synthesis and biological evaluation of 5-fluoroquinolone-3-carboxylic acids as potential HIV-1 integrase inhibitors. *J. Enzym. Inhib. Med. Chem.* **2012**, *28*, 671–676. [[CrossRef](#)]
42. Malík, M.; Tlustoš, P. Nootropics as cognitive enhancers: Types, dosage and side effects of smart drugs. *Nutrients* **2022**, *14*, 3367. [[CrossRef](#)]
43. Stankevich, M.I.; Stankevich, I.V.; Zefirov, N.S. Topological indices in Organic Chemistry. *Russ. Chem. Rev.* **1998**, *57*, 191–208. [[CrossRef](#)]
44. Kajdas, C. General approach to mechanochemistry and its relation to tribochemistry. *Tribol. Eng.* **2013**, *11*, 209–230.
45. Maeda, Y.; Kiba, A.; Ohnishi, K.; Hikichi, Y. Implications of amino acid substitutions in GyrA at position 83 in terms of oxolinic acid resistance in field isolates of *Burkholderia glumae*, a causal agent of bacterial seedling rot and grain rot of Rice. *Appl. Environ. Microbiol.* **2004**, *70*, 5613–5620. [[CrossRef](#)] [[PubMed](#)]
46. Tang, K.; Zhao, H. Quinolone antibiotics: Resistance and therapy. *Infect. Drug Resist.* **2023**, *16*, 811–820. [[CrossRef](#)] [[PubMed](#)]
47. Shaheen, A.; Tariq, A.; Iqbal, M.; Mirza, O.; Haque, A.; Walz, T.; Rahman, M. Mutational diversity in the quinolone resistance-determining regions of type-II topoisomerases of salmonella serovars. *Antibiotics* **2021**, *10*, 1455. [[CrossRef](#)] [[PubMed](#)]
48. Mehla, K.; Ramana, J. Structural signature of Ser83Leu and Asp87Asn mutations in DNA gyrase from enterotoxigenic *Escherichia coli* and impact on quinolone resistance. *Gene* **2016**, *576*, 28–35. [[CrossRef](#)] [[PubMed](#)]
49. Liu, J.; Zhang, H.; Xiao, Z.; Wang, F.; Wang, X.; Wang, Y. Combined 3D-QSAR, Molecular Docking and Molecular Dynamics Study on Derivatives of Peptide Epoxyketone and Tyropeptin-Boronic Acid as Inhibitors Against the $\beta 5$ Subunit of Human 20S Proteasome. *Int. J. Mol. Sci.* **2011**, *12*, 1807–1835. [[CrossRef](#)] [[PubMed](#)]
50. Li, L.; Ji, J.; Song, F.; Hu, J. Intercellular receptor-ligand binding: Effect of protein-membrane interaction. *J. Mol. Biol.* **2023**, *435*, 167787. [[CrossRef](#)]
51. Min, X.; Cheng, S.; Jincui, Y.; Qing, W.; Niu, H. Systematic Investigation of Docking Failures in Large-Scale Structure-Based Virtual Screening. *ACS Omega* **2022**, *7*, 39417–39428.
52. Quiroga, R.; Villarreal, M. Vinardo: A Scoring Function Based on Autodock Vina Improves Scoring, Docking, and Virtual Screening. *PLoS ONE* **2016**, *11*, e0155183. [[CrossRef](#)]
53. Sulimov, V.B.; Sulimov, A.V. *Docking: Molecular Modeling for Drug Discovery*; AINTELL: Moscow, Russia, 2017; p. 348.
54. Suvannang, N.; Nantasenamat, C.; Isarankura-Na-Ayudhya, C.; Prachayasittikul, V. Molecular Docking of Aromatase Inhibitors. *Molecules* **2011**, *16*, 3597–3617. [[CrossRef](#)]
55. Novichikhina, N.P.; Shestakov, A.S.; Medvedeva, S.M.; Lagutina, A.M.; Krysin, M.Y.; Podoplelova, N.A.; Panteleev, M.A.; Ilin, I.S.; Sulimov, A.V.; Tashchilova, A.S.; et al. New Hybrid Tetrahydropyrrolo[3,2,1-ij]quinolin-1-ylidene-2-thioxothiazolidin-4-ones as New Inhibitors of Factor Xa and Factor XIa: Design, Synthesis, and In Silico and Experimental Evaluation. *Molecules* **2023**, *28*, 3851. [[CrossRef](#)]

Disclaimer/Publisher’s Note: The statements, opinions and data contained in all publications are solely those of the individual author(s) and contributor(s) and not of MDPI and/or the editor(s). MDPI and/or the editor(s) disclaim responsibility for any injury to people or property resulting from any ideas, methods, instructions or products referred to in the content.